Energy 60 (2013) 87–93

Contents lists available at ScienceDirect

Energy

journal homepage: www.elsevier.com/locate/energy

Fabrication and thermoelectric power of π-shaped $Ca_3Co_4O_9$/$CaMnO_3$ modules for renewable energy conversion

K. Park*, G.W. Lee

Faculty of Nanotechnology and Advanced Materials Engineering, Sejong University, Seoul 143-747, Republic of Korea

ARTICLE INFO

Article history:
Received 11 December 2012
Received in revised form
10 July 2013
Accepted 12 July 2013
Available online 24 August 2013

Keywords:
Thermoelectric module
Output powers
Thermoelectricity
Power generation

ABSTRACT

The thermoelectric modules of π-shaped 1-, 2-, and 4-pairs are constructed using p-type $Ca_{2.76}Cu_{0.24}Co_4O_9$ and n-type $Ca_{0.8}Dy_{0.2}MnO_3$ oxide materials. The reacted phases at the interfaces of the $Ca_{2.76}Cu_{0.24}Co_4O_9$/Ag electrode and $Ca_{0.8}Dy_{0.2}MnO_3$/Ag electrode are not observed. The output powers of the fabricated π-shaped modules are measured, depending on the operating parameters and number of thermoelectric module pairs. The output powers of single thermoelectric modules increase with an increase in temperature difference ΔT between the hot- and cold-side temperatures of the modules, i.e., 2.42, 3.65, 4.26, 5.70, 7.13, and 8.42 mW for $\Delta T = 250$, 269, 293, 305, 324, and 346 °C, respectively. The maximum output powers of 1-, 2-, and 4-pair thermoelectric modules are roughly proportional to the number of p-n pairs. Oxide-based thermoelectric devices can be considered useful tools for green energy generation.

1. Introduction

Dramatic progress has been made in recent years in the development of renewable energy technology that can reduce greenhouse gas emissions, fossil fuel usage, and environmental contamination. Thermoelectric devices can convert thermal energy, i.e., waste heat, into electrical power *via* the Seebeck effect [1–8]. The energy absorbed from external sources in the form of heat results in electron motion from a hot region to a cold region within the material [9]. Thermoelectric devices are composed of p- and n-type semiconductor legs that are connected electrically in series by metal strips and thermally in parallel [1,7,10–12]. Unlike conventional heat engines, a thermoelectric device is a solid-state energy converter, which does not contain moving parts and is compact and environmentally friendly [13–16]. Therefore, thermoelectric devices can be considered useful tools to practice green energy technology. However, the relatively low conversion efficiency of the thermoelectric modules (5%) has restricted their application in electrical power generation [17,18].

So far, Bi_2Te_3-based thermoelectric modules have been extensively studied and have been widely commercially available [19–21]. However, several works have investigated the fabrication and performance of oxide-based thermoelectric modules for power generation [22–25]. Shin et al. [22] reported the construction of oxide-based thermoelectric modules for power generation and their performance. The modules were assembled based on the p-type Li-doped NiO and n-type (Ba,Sr)PbO_3, along with the alumina fin as the thermal radiator. This oxide module was stable at a high temperature of 617 °C in air. The obtained results offered the design and manufacture of oxide-based thermoelectric modules. Subsequently, Funahashi et al. [23] fabricated a thermoelectric unicouple, which was composed of the p-type $Ca_{2.7}Bi_{0.3}Co_4O_9$ and n-type $La_{0.9}Bi_{0.1}NiO_3$ using Ag paste containing p- and n-type oxide powders. They proposed that the junctions acting as thermal and electrical buffer layers need to be constructed between two oxide legs and Ag on the alumina substrate. The addition of oxide powders into the Ag paste was highly effective in improving the performance of the modules. Noudem et al. [24] reported the fabrication of thermoelectric modules based on the p-type $Ca_3Co_4O_9$ and n-type $Ca_{0.95}Sm_{0.05}MnO_3$. The open porous foam structures of the thermoelectric materials were highly efficient for waste heat recovery due to the phonon confinement. Noudem et al. demonstrated a way to reduce the contact resistance and the feasibility to design the thermoelectric modules. More recently, Park et al. [25] constructed single thermoelectric modules, based on the p-type $Na(Co_{0.95}Ni_{0.05})_2O_4$ and n-type $Zn_{0.99}Sn_{0.01}O$, and then measured their thermoelectric properties. The output voltage of the thermoelectric modules enhanced linearly with the hot-side temperature of modules (T_h), while the output current exponentially increased with the T_h. It is known that the operating

* Corresponding author. Tel.: +82 2 3408 3777; fax: +82 2 3408 4342.
E-mail address: kspark@sejong.ac.kr (K. Park).

0360-5442/$ – see front matter © 2013 Elsevier Ltd. All rights reserved.
http://dx.doi.org/10.1016/j.energy.2013.07.025

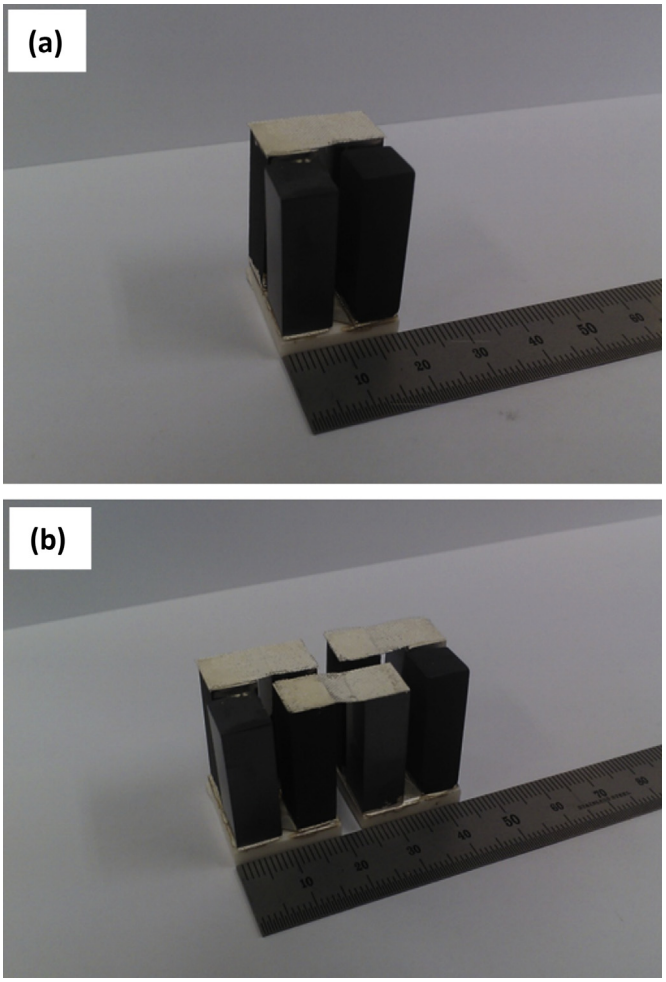

Fig. 1. Photographs of (a) two- and (b) four-pair π-shaped thermoelectric modules with Ag electrode.

parameter and number of module pairs affect the generated output performance. In the present study, the influence of the operating parameter and number of module pairs on the output power is investigated. Here the operating parameters include the T_h, the cold-side temperature of modules (T_c), and the temperature difference between the T_h and T_c (ΔT).

2. Experimental method

The semiconducting $Ca_{2.76}Cu_{0.24}Co_4O_9$ and $Ca_{0.8}Dy_{0.2}MnO_3$ ceramics were fabricated by the solid-state reaction method, using solution-combustion-processed $Ca_{2.76}Cu_{0.24}Co_4O_9$ and $Ca_{0.8}Dy_{0.2}MnO_3$ powders. Further details on the fabrication of $Ca_{2.76}Cu_{0.24}Co_4O_9$ and $Ca_{0.8}Dy_{0.2}MnO_3$ ceramics may be found elsewhere [26,27]. The morphological characteristics of $Ca_{2.76}Cu_{0.24}Co_4O_9$ and $Ca_{0.8}Dy_{0.2}MnO_3$ ceramics were investigated with a FE-SEM (field emission scanning electron microscope; Hitachi S4700). To fabricate the thermoelectric modules, which consisted of the p-type $Ca_{2.76}Cu_{0.24}Co_4O_9$ and n-type $Ca_{0.8}Dy_{0.2}MnO_3$ with dimensions of 7 mm × 9 mm × 25 mm, Ag paste was printed on connecting sections of the oxide legs and the alumina plate at 4 mm thickness. After joining the oxide legs and alumina plate, the joint was dried at 60 °C and then heated at 700 °C under a uniaxial pressure of 12.3 kPa in air to construct single π-shaped thermoelectric modules. In a similar way to single π-shaped modules, two- and four-pair π-shaped thermoelectric modules were constructed for higher output power (Fig. 1).

The interfaces at the $Ca_{2.76}Cu_{0.24}Co_4O_9$/Ag electrode and the $Ca_{0.8}Dy_{0.2}MnO_3$/Ag electrode were investigated by SEI (secondary electron image) and EDS (energy dispersive spectroscopy). To ensure the temperature difference in the thermoelectric modules, one side of the thermoelectric modules was heated with a hot plate, and the other side was cooled by running cold water in a rectangular pipe. To measure the temperatures of high- and low-temperature sides, the heads of the two K-type thermocouples were attached on the alumina plates of high- and low-temperature sides using a ceramic bond, respectively. A photograph of output power measurement of π-shaped thermoelectric module is shown in Fig. 2. The output power (W) was calculated by the output voltage (V) and current (I) caused by changing a small amount of current with a source meter (Keithley 2400).

3. Results and discussion

The temperature dependence of the thermoelectric properties of the p-type $Ca_{2.76}Cu_{0.24}Co_4O_9$ and n-type $Ca_{0.8}Dy_{0.2}MnO_3$ is shown in Fig. 3 [26,27]. The electrical conductivity of the two samples slightly increased with increasing temperature, indicating semiconducting behavior. The signs of the Seebeck coefficients of $Ca_{2.76}Cu_{0.24}Co_4O_9$ and $Ca_{0.8}Dy_{0.2}MnO_3$ are positive and negative, respectively, over the measuring temperature range, indicating p- and n-type conductions, respectively. The highest power factors of $Ca_{2.76}Cu_{0.24}Co_4O_9$ and $Ca_{0.8}Dy_{0.2}MnO_3$ are 3.8×10^{-4} Wm^{-1} K^{-2} and 3.7×10^{-5} Wm^{-1} K^{-2} at 800 °C, respectively. The power factor

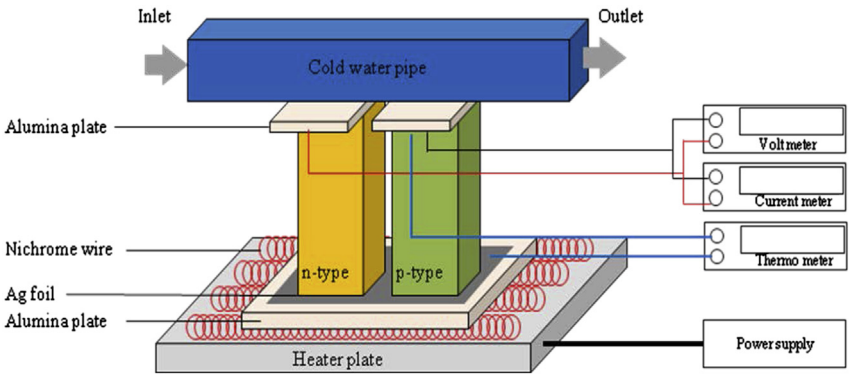

Fig. 2. A schematic diagram of the apparatus for the output power measurement.

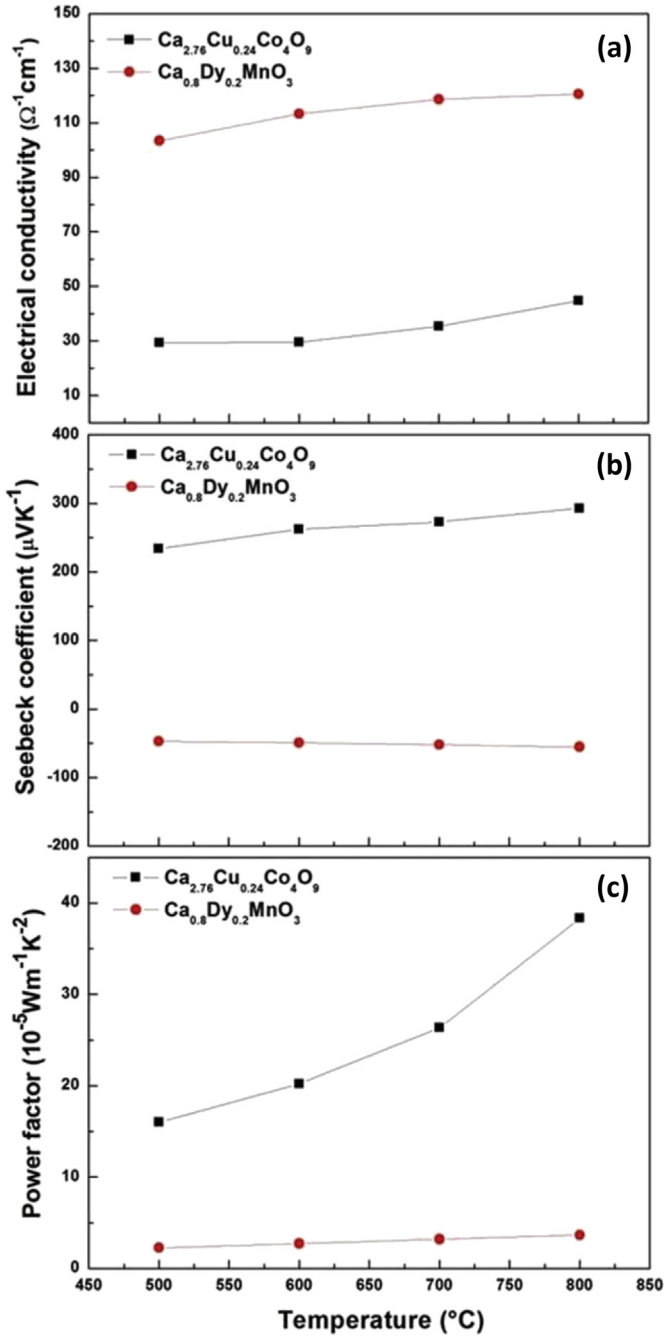

Fig. 3. Temperature dependence of the (a) electrical conductivity, (b) Seebeck coefficient, and (c) power factor of p-type $Ca_{2.76}Cu_{0.24}Co_4O_9$ and n-type $Ca_{0.8}Dy_{0.2}MnO_3$.

of $Ca_{2.76}Cu_{0.24}Co_4O_9$ is about ten times higher than that of $Ca_{0.8}Dy_{0.2}MnO_3$.

In an attempt to understand the diffusion of constituents in the p-type $Ca_{2.76}Cu_{0.24}Co_4O_9$ and Ag electrode, the amount of constituent elements near the interface between the two components was investigated by EDS. A cross-sectional SEI and EDS spectrum from the interface between the $Ca_{2.76}Cu_{0.24}Co_4O_9$ and Ag electrode are shown in Fig. 4. The thickness of the Ag electrode was ~20 μm. No reacted phase at the interface was observed. Good interfacial joining between the two components is essential for the practical applications of thermoelectric modules [23].

The Ag element in the electrode was scarcely diffused into the p-type material, whereas a very small amount of Ca, Cu, Co, and O elements in the p-type material was diffused into the Ag electrode. Fig. 5 shows a cross-sectional SEI and EDS spectra from the interface between the n-type $Ca_{0.8}Dy_{0.2}MnO_3$ and Ag electrode. The thickness of the Ag electrode was ~27 μm, and no reacted phase was detected at the interface. Small amounts of Ag in the electrode and Ca, Dy, Mn, and O in the n-type material were detected in the n-type material and the Ag electrode, respectively.

The mismatch in the CTE (coefficient of thermal expansion) between the oxide leg and electrode results in the generation of residual stresses after fabrication. Fig. 6 shows the CTE of the $Ca_{2.76}Cu_{0.24}Co_4O_9$ and $Ca_{0.8}Dy_{0.2}MnO_3$ used as oxide legs and alumina at 300–800 °C. The CTE (β) is defined as [28]:

$$\beta = \frac{L_f - L_0}{L_0\left(T_f - T_0\right)} = \frac{\Delta L}{L_0 \Delta T} \tag{1}$$

where L_f, L_0, T_f, and T_0 are the final length, initial length, final temperature, and initial temperature of samples, respectively. The CTEs at 800 °C for $Ca_{2.76}Cu_{0.24}Co_4O_9$ and $Ca_{0.8}Dy_{0.2}MnO_3$, calculated from Eq. (1), are 1.12×10^{-5} and 1.16×10^{-5} K^{-1}, respectively. The CTEs at 400 and 1000 °C for alumina are 0.74×10^{-5} and 0.83×10^{-5} K^{-1}, respectively [29]. Since the difference between the CTEs of $Ca_{0.8}Dy_{0.2}MnO_3$ and alumina is higher than that of $Ca_{2.76}Cu_{0.24}Co_4O_9$ and alumina, the residual stress generated at the joint of $Ca_{0.8}Dy_{0.2}MnO_3$/alumina is larger than that of $Ca_{2.76}Cu_{0.24}Co_4O_9$/alumina. The residual stress (η), caused by restricting thermal expansion, can be written as [30]:

$$\eta = \beta E \Delta T \tag{2}$$

where E is the Elastic modulus and ΔT is the temperature difference. No cracks were observed at the joints of the $Ca_{2.76}Cu_{0.24}Co_4O_9$/alumina and $Ca_{0.8}Dy_{0.2}MnO_3$/alumina after fabrication.

The I–V and I–W curves of π-type unit thermoelectric module were obtained under different T_c, T_h, and ΔT. Fig. 7 shows the I–V and I–W curves of π-type unit thermoelectric module as a function of temperature difference ΔT at $T_h = 380$ °C. The maximum power output (P_{max}) of the modules can be calculated by the following equation:

$$P_{max} = \frac{V_0^2}{4R_{in}} \tag{3}$$

where V_0 and R_{in} are the open circuit voltage and the internal resistance, respectively. Without the cold running water, the temperature difference ΔT was as large as 190 °C. The open circuit voltage and maximum output power at $\Delta T = 190$ °C were 31.4 mV and 1.25 mW, respectively. On the other hand, when the cold water ran in the rectangular pipe, ΔT was 265 °C. The open circuit voltage and the maximum output power at $\Delta T = 265$ °C were 43.8 mV and 2.42 mW, respectively.

In addition, we obtained the I–V and I–W curves of the π-type unit thermoelectric module at different hot-side temperature, $T_h = 530$ °C, as a function of ΔT, as shown in Fig. 8. Without running the cold water, the temperature difference ΔT was as large as 215 °C. The open circuit voltage and maximum output power at $\Delta T = 215$ °C were 41.4 mV and 2.39 mW, respectively. On the other hand, when the cold water ran in the rectangular pipe, ΔT was 260 °C. The open circuit voltage and maximum output power were 50.1 mV and 3.75 mW, respectively. In addition to the T_c, T_h, and ΔT discussed previously, we obtained the I–V and I–W curves of single thermoelectric modules under different operating parameters.

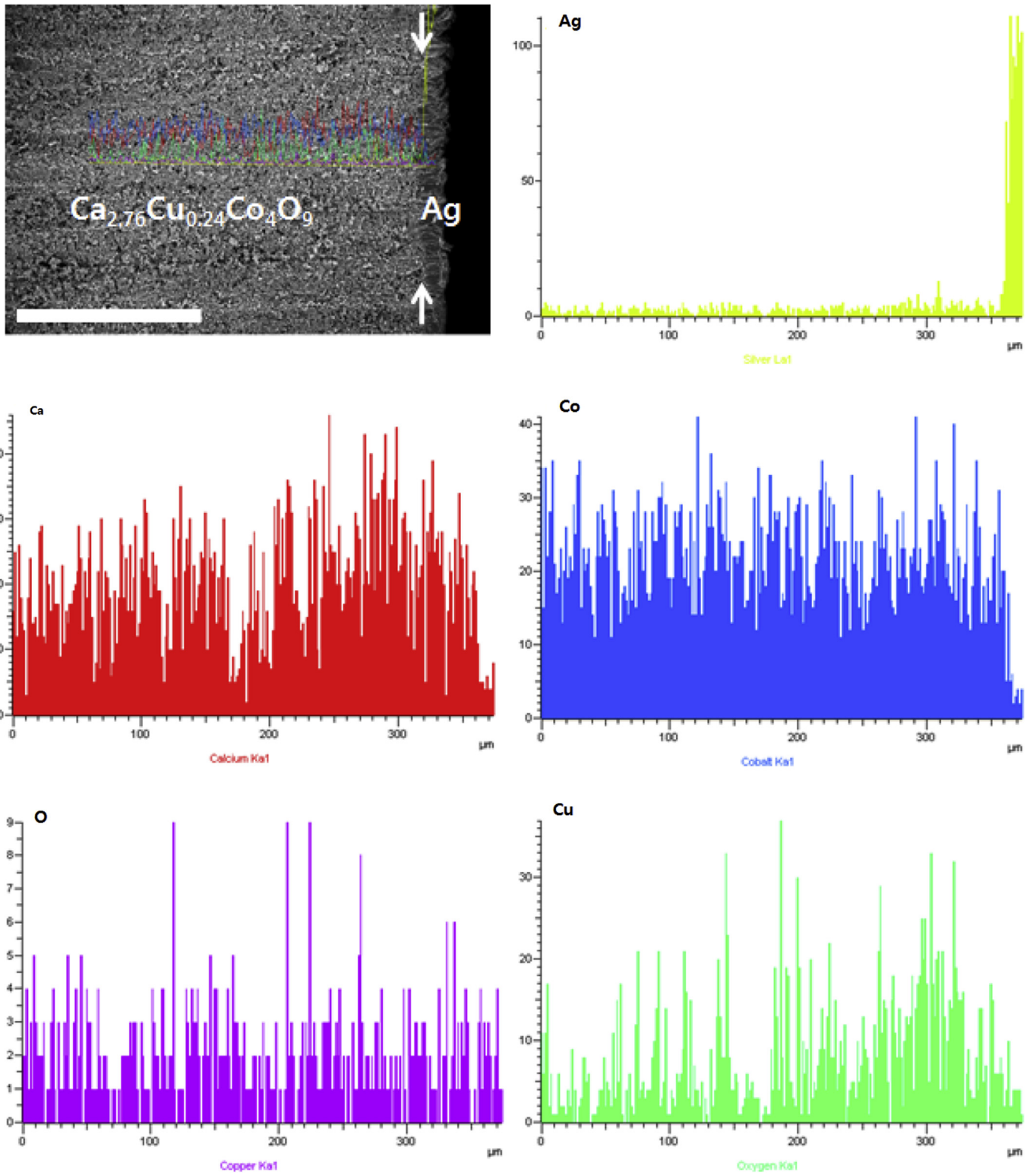

Fig. 4. A cross-sectional SEI and EDS spectrum from the interface between the $Ca_{2.76}Cu_{0.24}Co_4O_9$ and Ag electrode.

Prior to the measurement of output power, at a given hot-side temperature T_h, the temperature difference ΔT was measured, as shown in Fig. 9. The temperature difference is roughly proportional to the hot-side temperature. The maximum output powers of the thermoelectric unit modules under various operating parameters are given in Table 1. The output powers increase with increasing temperature difference ΔT, i.e., 2.42, 3.65, 4.26, 5.70, 7.13, and 8.42 mW for $\Delta T = 250, 269, 293, 305, 324$, and 346 °C, respectively.

In order to increase the generated output voltage, π-shaped two- and four-pair thermoelectric modules were connected electrically in series each other and thermally in parallel. When n is the number of modules in series, the output voltage of thermoelectric

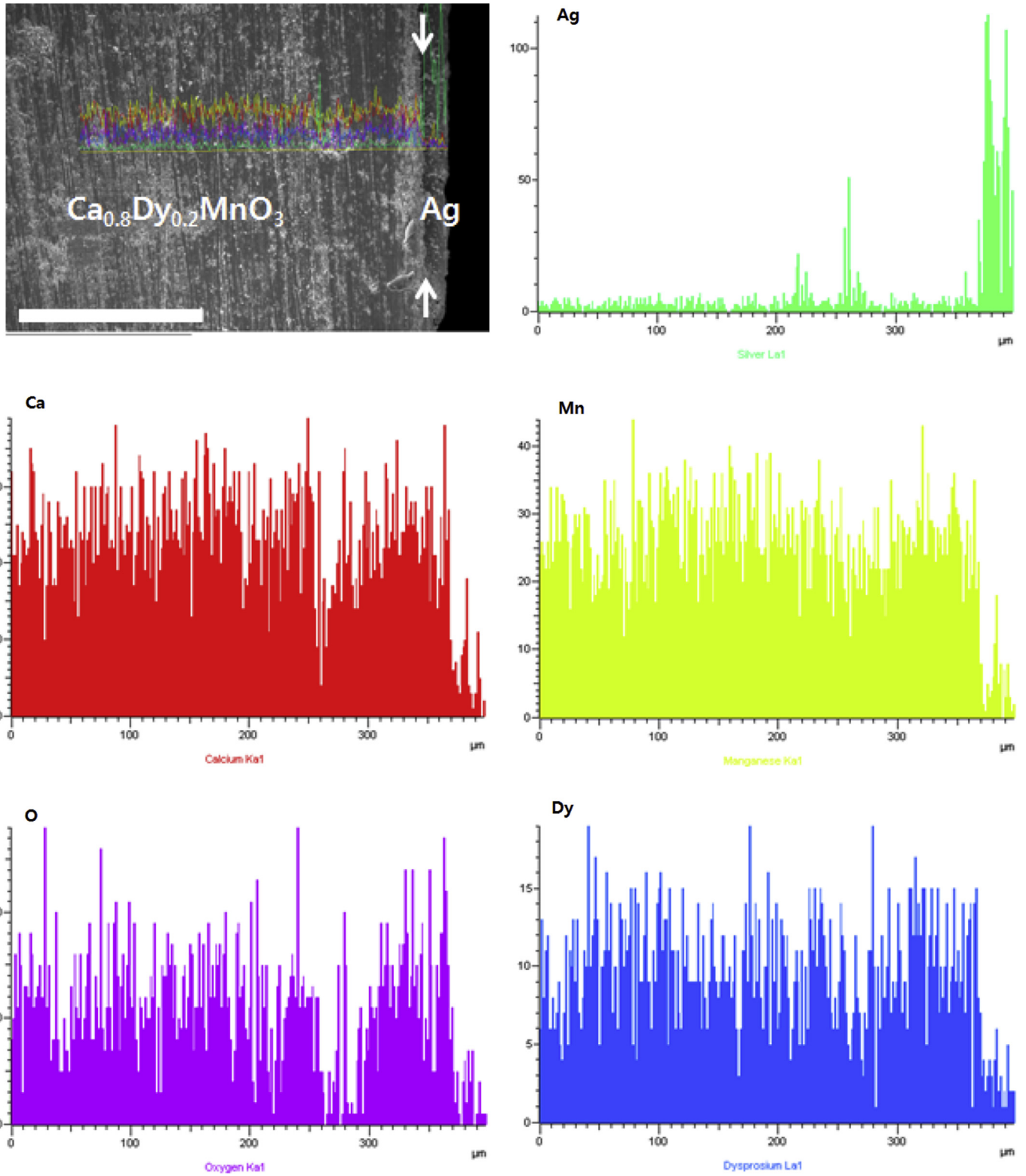

Fig. 5. A cross-sectional SEI and EDS spectrum from the interface between the n-type $Ca_{0.8}Dy_{0.2}MnO_3$ and Ag electrode.

modules can theoretically generate n times larger than that of the unit module. Fig. 10 shows the I–V and I–W curves of a two-pair thermoelectric module under $T_h = 594$ °C and $\Delta T = 311$ °C. The open circuit voltage and maximum output power were 138 mV and 16.14 mW, respectively. Although the temperature difference in the two-pair thermoelectric module ($\Delta T = 311$ °C) shown in Fig. 10 is similar to that in the single thermoelectric module ($\Delta T = 305$ °C) given in Table 1, the maximum output power of two-pair module (16.14 mW) is over two times larger than that of a π-type unit module (5.7 mW). This may be due to the fact that the contact

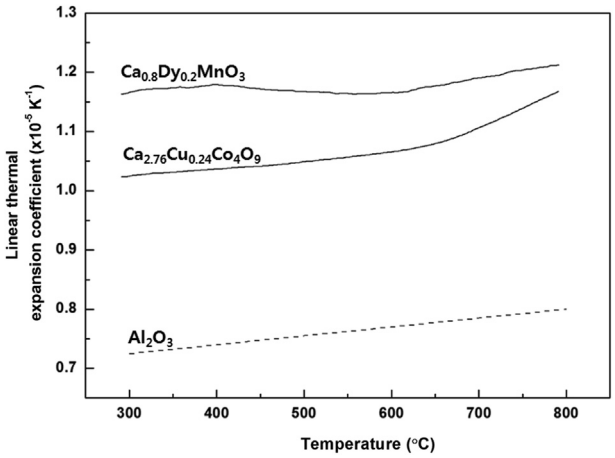

Fig. 6. CTE of the $Ca_{2.76}Cu_{0.24}Co_4O_9$ and $Ca_{0.8}Dy_{0.2}MnO_3$ used as oxide legs and alumina at 300–800 °C.

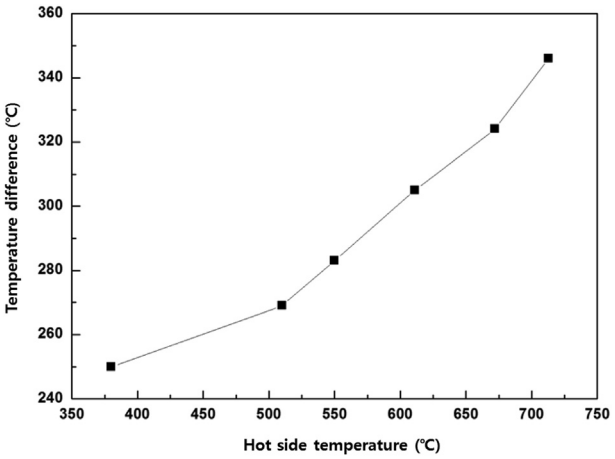

Fig. 9. Relationship between temperature difference and hot-side temperature of π-type unit thermoelectric module.

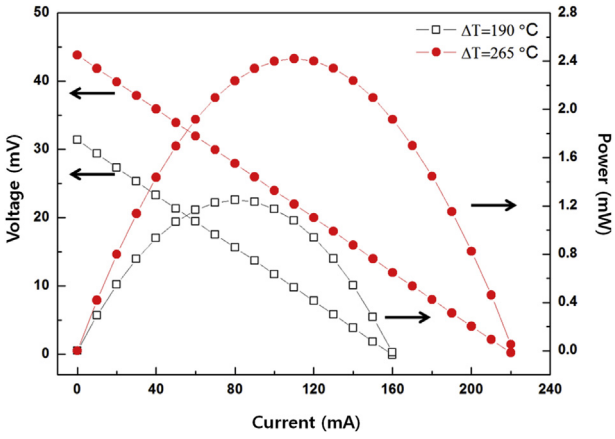

Fig. 7. *I–V* and *I–W* curves of π-type unit thermoelectric module as a function of temperature difference at T_h = 380 °C.

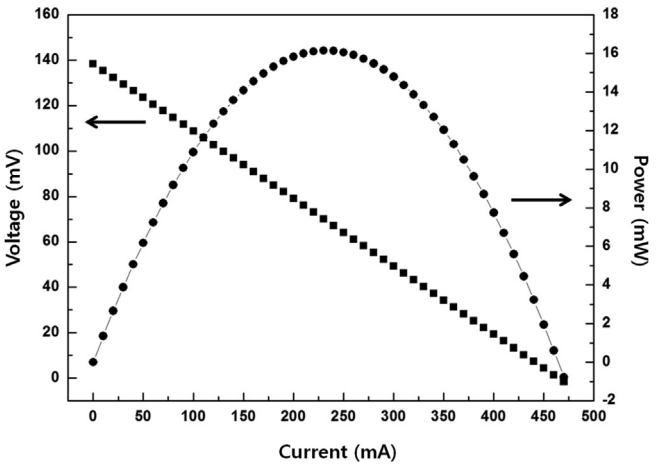

Fig. 10. *I–V* and *I–W* curves of two-pair thermoelectric module under T_h = 594 °C and ΔT = 311 °C.

resistance in a single thermoelectric module is larger than that in a two-pair thermoelectric module.

The *I–V* and *I–W* curves of a four-pair thermoelectric module under T_h = 664 °C and ΔT = 321 °C are shown in Fig. 11. The measured open circuit voltage and maximum output power are 282 mV and 31.12 mW, respectively. A summary of the maximum output powers of the 1-, 2-, and 4-pair modules discussed previously is shown in Fig. 12. The maximum output power was roughly proportional to the number of the p-n pairs. The module was stable enough to operate at high temperature. No crack was detected inside the module after measuring the output power. Based on the above results, thermoelectric power generation can be considered one of the alternative renewable energy resources.

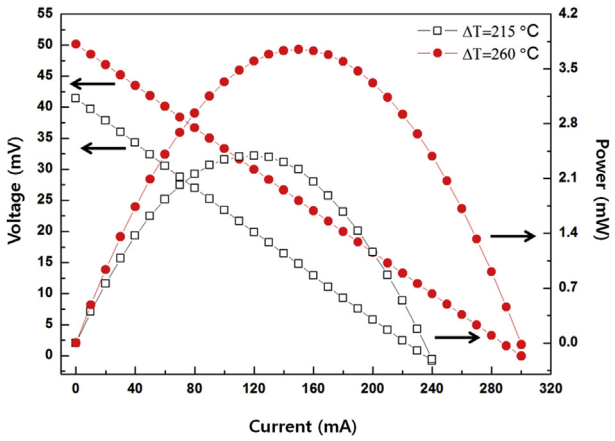

Fig. 8. *I–V* and *I–W* curves of π-type unit thermoelectric module as a function of temperature difference at T_h = 530 °C.

Table 1
Maximum output powers of the thermoelectric unit modules under various operating parameters.

Hot side temperature (T_h, °C)	Cold side temperature (T_c, °C)	Temperature difference (T_h–T_c, °C)	Open circuit voltage (mV)	Maximum output power (mW)
80	130	250	43.8	2.42
510	241	269	50.7	3.65
550	257	293	56.3	4.26
611	306	305	64.4	5.70
672	348	324	71.1	7.13
713	367	346	77.3	8.42

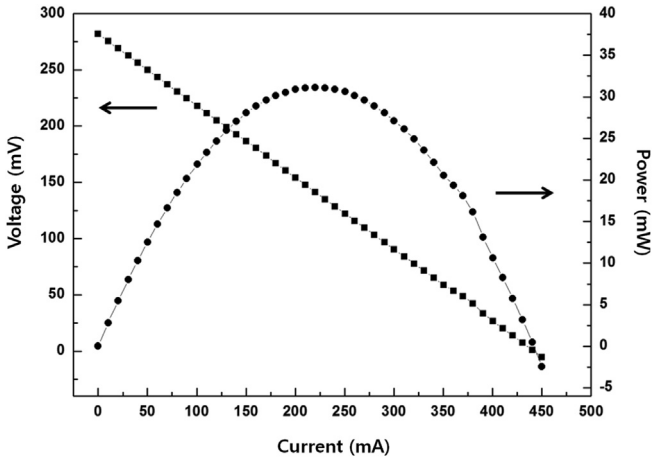

Fig. 11. *I–V* and *I–W* curves of four-pair thermoelectric module under $T_h = 664$ °C and $\Delta T = 321$ °C.

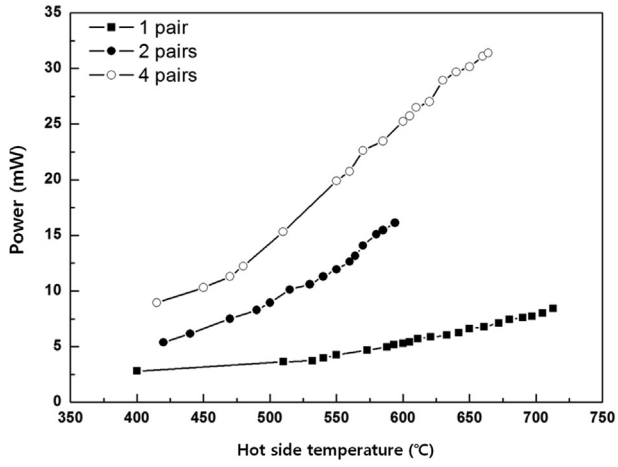

Fig. 12. Maximum output powers of 1-, 2-, and 4-pair modules as a function of hot-side temperature.

4. Conclusions

Oxide-based thermoelectric modules, based on p-type $Ca_{2.76}Cu_{0.24}Co_4O_9$ and n-type $Ca_{0.8}Dy_{0.2}MnO_3$, were fabricated. No reacted phase was detected at the interfaces between the p-type $Ca_{2.76}Cu_{0.24}Co_4O_9$/Ag electrode and n-type $Ca_{0.8}Dy_{0.2}MnO_3$/Ag electrode. The output powers of single thermoelectric modules under temperature difference $\Delta T = 250$, 269, 293, 305, 324, and 346 °C were 2.42, 3.65, 4.26, 5.70, 7.13, and 8.42 mW, respectively. This indicated that the output powers increased with the increasing temperature difference. The maximum output powers of 1-, 2-, and 4-pair modules were roughly proportional to the number of p-n pairs. Hence, thermoelectric power generation can be considered one of alternative renewable energy resources.

Acknowledgment

This research was supported by Basic Science Research Program through the National Research Foundation of Korea (NRF) funded by the Ministry of Education, Science and Technology (2012R1A1A2009194).

References

[1] Hsu CT, Huang GY, Chu HS, Yu B, Yao DJ. An effective seebeck coefficient obtained by experimental results of a thermoelectric generator module. Applied Energy 2011;88:5173–9.
[2] Rowe DM. Applications of nuclear-powered thermoelectric generators in space. Applied Energy 1991;40:241–71.
[3] Xiao J, Yang T, Li P, Zhai P, Zhang Q. Thermal design and management for performance optimization of solar thermoelectric generator. Applied Energy 2012;93:33–8.
[4] Champier D, Bédécarrats JP, Kousksou T, Rivaletto M, Strub F, Pignolet P. Study of a TE (thermoelectric) generator incorporated in a multifunction wood stove. Energy 2011;36:1518–26.
[5] Barati M, Esfahani S, Utigard TA. Energy recovery from high temperature slags. Energy 2011;36:5440–9.
[6] Cheng TC, Cheng CH, Huang ZZ, Liao GC. Development of an energy-saving module via combination of solar cells and thermoelectric coolers for green building applications. Energy 2011;36:133–40.
[7] Sahin AZ, Yilbas BS. Thermodynamic irreversibility and performance characteristics of thermoelectric power generator. Energy 2013;55:899–904.
[8] Park K, Hwang HK, Seo JW, Seo WS. Enhanced high-temperature thermoelectric properties of Ce- and Dy-doped ZnO for power generation. Energy 2013;54:139–45.
[9] Yilbas BS, Sahin AZ. Thermoelectric device and optimum external load parameter and slenderness ratio. Energy 2010;35:5380–4.
[10] Pan Y, Lin B, Chen J. Performance analysis and parametric optimal design of an irreversible multi-couple thermoelectric refrigerator under various operating conditions. Applied Energy 2007;84:882–92.
[11] Meng F, Chen L, Sun F. A numerical model and comparative investigation of a thermoelectric generator with multi-irreversibilities. Energy 2011;36:3513–22.
[12] Jang JY, Tsai YC, Wu CW. A study of 3-D numerical simulation and comparison with experimental results on turbulent flow of venting flue gas using thermoelectric generator modules and plate fin heat sink. Energy 2013;53:270–81.
[13] Wang CC, Hung CI, Chen WH. Design of heat sink for improving the performance of thermoelectric generator using two-stage optimization. Energy 2012;39:236–45.
[14] Sahin AZ, Yilbas BS, Shuja SZ, Momin O. Investigation into topping cycle: thermal efficiency with and without presence of thermoelectric generator. Energy 2011;36:4048–54.
[15] Gou X, Yang S, Xiao H, Ou Q. A dynamic model for thermoelectric generator applied in waste heat recovery. Energy 2013;52:201–9.
[16] Chen WH, Liao CY, Hung CI, Huang WL. Experimental study on thermoelectric modules for power generation at various operating conditions. Energy 2012;45:874–81.
[17] Rowe DW, Min G. Evaluation of thermoelectric modules for power generation. Journal of Power Sources 1998;73:193–8.
[18] Yu J, Zhao H. A numerical model for thermoelectric generator with the parallel-plate heat exchanger. Journal of Power Sources 2007;172:428–34.
[19] Wang S, Xie W, Li H, Tang X. Enhanced performances of melt spun $Bi_2(Te, Se)_3$ for n-type thermoelectric legs. Intermetallics 2011;19:1024–31.
[20] Nakagiri Y, Gyoten H, Yamamoto Y. Development of film-shaped thermoelectric materials for thermoelectric modules. Applied Energy 1998;59:147–62.
[21] Huang C, Christou A. Diffusion controlled degradation analysis of high temperature $(Bi, Sb)_2(Te, Se)_3$ semiconductor thermoelectric power modules. Materials Science and Engineering: B 1995;29:233–6.
[22] Shin W, Murayama N, Ikeda K, Sago S. Thermoelectric power generation using Li-doped NiO and (Ba, Sr)PbO_3 module. Journal of Power Sources 2001;103:80–5.
[23] Funahashi R, Urata S, Mizuno K, Kouuchi T, Mikami M. $Ca_{2.7}Bi_{0.3}Co_4O_9/La_{0.9}Bi_{0.1}NiO_3$ thermoelectric devices with high output power density. Applied Physics Letters 2004;85:1036–8.
[24] Noudem JG, Lemonnier S, Prevel M, Reddy ES, Guilmeau E, Goupil C. Thermoelectric ceramics for generators. Journal of the European Ceramic Society 2008;28:41–8.
[25] Park K, Choi JW, Lee CW. Characteristics of thermoelectric power modules based on p-type $Na(Co_{0.95}Ni_{0.05})_2O_4$ and n-type $Zn_{0.99}Sn_{0.01}O$. Journal of Alloys and Compounds 2009;486:785–9.
[26] Park K, Lee G. Thermoelectric properties of $Ca_{0.8}Dy_{0.2}MnO_3$ synthesized by solution combustion process. Nanoscale Research Letters 2011;6:548.
[27] Lee GW, Kim JY, Athar T, Kim SJ, Seo WS, Park K. Electrical conductivity and thermoelectric power studies of solution-combustion-processed $Ca_{2.76}Cu_{0.24}Co_4O_9$. Ceramics International 2013;39:1397–402.
[28] Uršič H, Malič B, Cilenšek J, Rojac T, Kmet B, Kosec M. Linear thermal expansion coefficients of relaxor-ferroelectric $0.57Pb(Sc_{1/2}Nb_{1/2})O_3$–$0.43PbTiO_3$ ceramics in a wide temperature range. Journal of the European Ceramic Society 2013;33:2167–71.
[29] Schneider Jr SJ. Engineered materials handbookIn Ceramics and glasses, vol. 4. ASM International; 1991.
[30] Lanin AG, Deryavko II. Influence of residual stresses on thermal stress resistance of refractory ceramic. Journal of the European Ceramic Society 2000;20:209–13.